Polarization Properties of Interferometrically Interrogated Fiber Bragg Grating and Tandem-Interferometer Strain Sensors

Geoffrey A. Cranch, Gordon M. H. Flockhart, and Clay K. Kirkendall, *Member, IEEE*

***Abstract*—Lead sensitivity in low-coherence interferometric fiber-optic sensors is a well-known problem. It can lead to a severe degradation in the sensor resolution and accuracy through its effect on the fringe visibility and interferometric phase. These sensitivities have been attributed to birefringence in the various components. In the current work, an analysis of the polarization properties of fiber Bragg grating and tandem-interferometer strain sensors, using Stokes calculus and the Poincaré sphere, is presented. The responses of these sensors as a function of the birefringence properties of the various components under different illuminating conditions are derived. The predicted responses demonstrate very good agreement with experimentally measured responses. These models provide a clear insight into the evolution of the polarization states through the sensor networks. Methods to overcome the lead sensitivity are discussed and demonstrated, which yield a differential strain measurement accuracy of 18 nε · rms for a fiber Bragg grating sensor.**

***Index Terms*—Birefringence, optical-fiber polarization, optical interferometry, optical noise, strain measurement.**

I. Introduction

WHITE-LIGHT interferometric interrogation of fiber Bragg grating (FBG) strain sensors has been demonstrated as a high-resolution method of decoding the strain-induced change in Bragg resonance for both single [1] and multiplexed [2] sensors. White-light tandem interferometry has also been applied to coherence multiplexed extrinsic fiber Fabry–Pérot (FFP) strain sensors [3] and time division multiplexed FBG FP sensors [4]. These sensor systems utilize a decoding interferometer to recover the signal from the optical sensor. In the case of the FBG sensor, the decoding interferometer converts the change in wavelength of the light reflected from the sensor to a change in intensity. In the white-light tandem interferometer, the decoding interferometer balances the optical path length of the light reflected from the sensing interferometer, yielding an interference signal, which contains the strain information of interest. It has been noted previously that the output of a tandem-interferometer arrangement can exhibit strong sensitivities to perturbations of the lead connecting the two interferometers [5]. This sensitivity manifests itself as fluctuations of both the output fringe visibility and interferometric phase. Changes in fringe visibility cause variation in the signal-to-noise ratio and, hence, self-noise of the sensor, whereas phase errors result in strain measurement errors. Lead sensitivity is observed for both polarized and unpolarized illumination to varying degrees. Gauthier *et al.* showed that this sensitivity arises due to the presence of birefringence in the decoding and sensing interferometers. They applied the Jones calculus to the tandem interferometer to infer how the birefringence can affect the fringe visibility and output phase for the case of a polarized illuminating source. This lead sensitivity is also common to the FBG sensor; however, to the best of the author's knowledge, no rigorous study has previously been presented. In this case perturbations of the lead connecting the decoding interferometer to the FBG sensor can give rise to fluctuations of the fringe visibility and output phase of the interferometer when birefringence is present in the network. Most optical fibers exhibit some intrinsic birefringence, and birefringence can be generated in the FBG during the writing process [6] or during the mounting procedure.

Techniques to overcome these lead-sensitivity effects have since been demonstrated, such as use of ortho-conjugate mirrors in the sensing interferometer [7]. Also, scrambling the birefringence in the lead connecting the two interferometers has been suggested as a method to remove this sensitivity [8]. An understanding of the origins of these sensitivities and a means to quantify them is particularly important for the successful operation of interferometrically interrogated differential strain sensors [9].

The present work examines the polarization properties of both the FBG and tandem-interferometer sensors. We show that by applying the Stokes calculus and through the use of the Poincaré-sphere representation of polarized light, the exact response of these two sensor systems when illuminated with polarized, unpolarized, and partially polarized light can be deduced. This is relevant to many systems since broadband sources often produce unpolarized light or can be depolarized with a Lyot depolarizer. Expressions for the fringe visibility and output phase for both sensors are derived, which include the effects of birefringence in the decoding interferometer, connecting lead, and sensing interferometer or FBG. These provide measurable quantities that are compared with experimental measurements to validate the model. This analysis provides a greatly improved understanding of the properties of these sensor systems and indicates the permissible levels of birefringence given a particular performance criterion.

Manuscript received August 18, 2005; revised January 10, 2006. This work was supported by the Office of Naval Research.

The authors are with SFA Inc., Crofton, MD, based at the Naval Research Laboratory, Washington, DC 20375 USA (e-mail: geoff.cranch@nrl.navy.mil).

Digital Object Identifier 10.1109/JLT.2006.871055

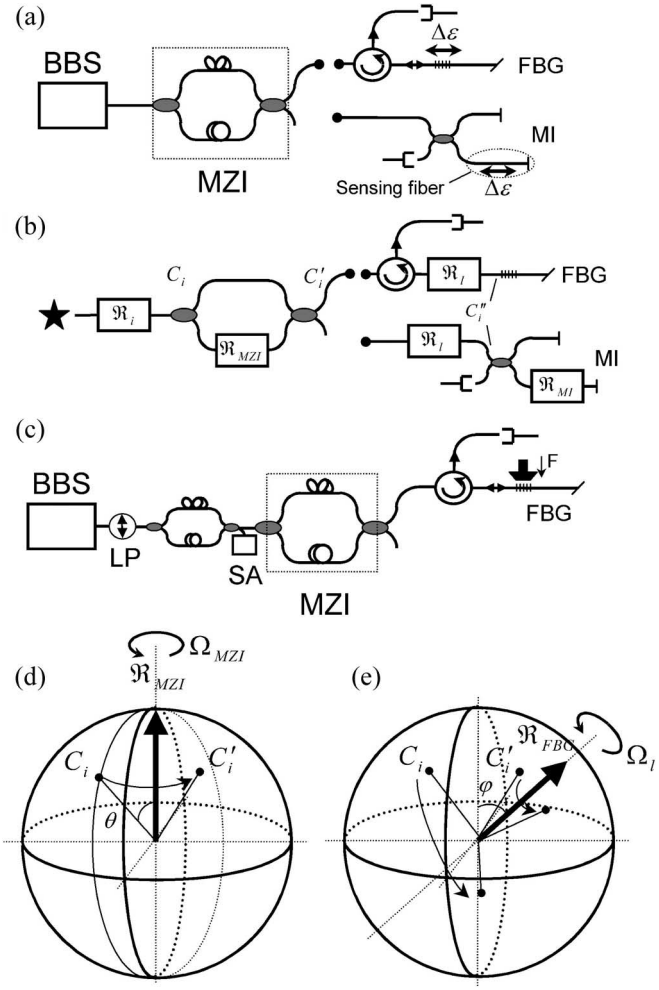

Fig. 1. (a) Typical arrangement of an FBG or MI strain sensor system, (b) equivalent birefringent network of the sensor systems, (c) FBG sensor with input DOP control, (d) Poincaré-sphere representation of the input and output polarization states of the MZI, and (e) Poincaré-sphere representation of the input and output polarization states of the FBG.

The manuscript is arranged as follows. Section II outlines the principles of interferometrically interrogated FBGs and tandem-interferometer arrangements. Section III presents the birefringence model for the FBG sensors and discusses the sensor response under various illumination conditions. Experimental measurements are then presented. Section IV applies the same model to the tandem-interferometer arrangement. Section V discusses the techniques that can be used to improve the sensor performance, and finally, the conclusions are summarized in Section VI. Please note that the equations derived in the appendices are labeled (A^*) or (B^*).

II. Interferometric Interrogation

A typical arrangement of the interferometrically interrogated FBG sensor is shown in Fig. 1(a). The emission from a broadband source is injected into a Mach–Zehnder interferometer (MZI). The output propagates along a connecting lead through an optical circulator and is reflected by the FBG to be separated on return through the circulator. The FBG narrows the optical spectrum, such that an interference signal is generated. An interrogation approach, such as phase-generated carrier or pseudo-heterodyne detection, is used to extract the interferometric phase. If the system is lossless, and the coupler ratios are exactly 50%, the output intensity is given by

$$I = \frac{R}{2} I_0 \left(1 + V \cos(\phi_{\mathrm{MZI}} + \phi_{\mathrm{FBG}})\right) \tag{1}$$

where I_0 is the input intensity, R is the power reflectivity of the FBG, V is a fringe-visibility term described below, and ϕ_{MZI} and ϕ_{FBG} are phase shifts associated with the MZI and FBG, respectively. Phase shifts in the MZI may arise from temperature changes or vibration and acoustics. These phase shifts can be rejected by interrogating a second FBG with the remaining output of the MZI and measuring the difference in phase between the two outputs [1]. The component of the measured phase associated with the FBG is related to the applied strain $\Delta\varepsilon$ by

$$\Delta\phi_{\mathrm{FBG}} = \frac{2\pi n d_{\mathrm{MZI}}}{\lambda_B}(0.78)\Delta\varepsilon \tag{2}$$

where n is the effective refractive index of the fiber, d_{MZI} is the path imbalance in the MZI, λ_B is the Bragg wavelength of the FBG, and the factor of 0.78 takes into account the stress-optic effect [10]. If the MZI is free from birefringence, then the fringe visibility is given by $V = \exp(-\tau^2/4\tau_c^2)$, where $\tau = n d_{\mathrm{MZI}}/c$ is the differential time delay, and $\tau_c = 1/(4\pi\Delta f)$ is the coherence time of the light reflected from the FBG. Δf is the rms half width of the reflected line shape, which for a Gaussian beam shape is related to the full-width half maximum $\Delta\lambda_{\mathrm{FWHM}}$ by $\Delta f = c\Delta\lambda_{\mathrm{FWHM}}/(4\sqrt{\ln 2}\lambda_B^2)$ [11]. For $\Delta\lambda_{\mathrm{FWHM}} = 0.2$ nm and $d_{\mathrm{MZI}} = 3$ mm, a visibility greater than 0.6 is obtained.

If the FBG is replaced with a Michelson interferometer (MI) and the optical path difference (OPD) in the MZI is balanced with the OPD of the MI, then the output intensity is

$$I = \frac{1}{2} I_0 \left(1 + \frac{V}{2}\cos(\phi_{\mathrm{MZI}} + \phi_{\mathrm{MI}})\right). \tag{3}$$

In practice, the OPD of the MI and MZI may not be exactly balanced, and the difference between the two is defined as the effective OPD of the system. The component of the measured phase associated with the MI is related to the applied strain $\Delta\varepsilon$ by

$$\Delta\phi_{\mathrm{MI}} = \frac{4\pi n d_{\mathrm{MI}}}{\lambda_B}(0.78)\Delta\varepsilon \tag{4}$$

where d_{MI} is the MI fiber length coupled to the strain. It is assumed that the bandwidth of the input radiation in the tandem interferometer is narrowed sufficiently to obtain coherent interference. Interference is observed when the coherence length of the input radiation is less than the effective OPD.

When birefringence is present in the interferometers and connecting leads, an extra multiplicative term must be included in the fringe visibility and an extra phase term added

to the interferometer phase to account for these polarization related effects. The remainder of this paper investigates these terms.

III. FBG Sensor

The interferometrically interrogated FBG sensor can be analyzed by utilizing the model presented by Kersey *et al.* [12], [13] for investigating the polarization properties of fiber-optic interferometers. In this model, the birefringence properties of the MZI are represented by a single birefringent element in one arm of the interferometer, as shown in Fig. 1(b); the other arm appearing isotropic to the propagating field. This element, denoted $\Re_{\mathrm{MZI}}(\Omega_{\mathrm{MZI}})$, is a 4×4 Mueller matrix and represents a general elliptic retarder of rotational magnitude (phase delay) Ω_{MZI}, which represents the "differential birefringence" in the MZI. The eigenvectors of this matrix represent the two eigenaxes of the MZI corresponding to orthogonal polarization axes. When an input state C_i is coincident with the eigenaxes of $\Re_{\mathrm{MZI}}$, it remains invariant in the transformation to C_i', and optimum fringe visibility is obtained. When C_i is not coincident with an eigenaxis, and subtends an angle θ to $\Re_{\mathrm{MZI}}$, it is transformed to a new state C_i'. This is represented on the Poincaré sphere as a rigid rotation about $\Re_{\mathrm{MZI}}$ by an angle Ω_{MZI}, as shown in Fig. 1(d). The birefringence in the input fiber is denoted $\Re_i$, and the birefringence in the connecting fiber is denoted $\Re_l(\Omega_l)$. In the current work, this model is extended to incorporate birefringence in the FBG and used to explain how sensitivities in the connecting leads arise for varying degrees of polarization of the incident light. The derivation of the general response of an FBG interrogated with polarized and unpolarized light is given in Appendix A. The remainder of this section will study the specific cases of this general response.

A. Illumination With Polarized Light

The general response of an FBG sensor illuminated with polarized light is given by (A3). The output intensity for an ideal birefringence-free FBG is given by setting $\Omega_{\mathrm{FBG}} = 0$ in (A3). This yields the equation for a birefringent fiber-optic interferometer illuminated with polarized light, as derived in [12], [13]

$$I = \frac{R}{2} I_0 \left(1 + \left\{ 1 - \sin^2\theta \sin^2\left(\frac{\Omega_{\mathrm{MZI}}}{2}\right)\right\}^{\frac{1}{2}} \times \cos\left(\Delta\phi_{\mathrm{FBG}}(\lambda_B) - \gamma\right)\right) \quad (5)$$

where $\tan\gamma = \tan(\Omega_{\mathrm{MZI}}/2)\cos\theta$. The fringe visibility V is therefore $\{1 - \sin^2\theta \sin^2(\Omega_{\mathrm{MZI}}/2)\}^{1/2}$. Thus, referring to Fig. 1(b), both the fringe visibility and interferometric phase depend on the birefringence properties of the MZI through Ω_{MZI} and input SOP: C_i through θ. In the absence of birefringence in the FBG, the fringe visibility and interferometric phase will be sensitive only to perturbations in the input fiber, which will change C_i.

Conversely, the case of the birefringence-free MZI with a birefringent FBG can be determined by setting $\Omega_{\mathrm{MZI}} = 0$ in (A3). This yields

$$I = \frac{R}{2} I_0 \cdot \left(1 + \left\{ 1 - \sin^2\varphi \sin^2\left(\frac{\Omega_{\mathrm{FBG}}}{2}\right)\right\}^{\frac{1}{2}} \times \cos\left(\Delta\phi(\bar{\lambda}) + \gamma\right)\right) \quad (6)$$

where $\tan\gamma = \tan(\Omega_{\mathrm{FBG}}/2)\cos\varphi$. $\bar{\lambda}$ is the mean wavelength of the FBG, and $\Omega_{\mathrm{FBG}} = 2\pi n d \Delta\lambda/\bar{\lambda}^2$ is related to the birefringence in the FBG; these are described further in Appendix A. The fringe visibility V is therefore $\{1 - \sin^2\varphi \sin^2(\Omega_{\mathrm{FBG}}/2)\}^{1/2}$. In this model, φ is the angle subtended by the birefringent axis of the FBG $\Re_{\mathrm{FBG}}$ to $\Re_{\mathrm{MZI}}$. On adding birefringence to the FBG, the visibility and phase become dependent on the birefringent properties of the FBG through Ω_{FBG} and input SOP to the FBG: C_i'' through φ. Birefringence in the input fiber will also change C_i''. Thus, perturbations to the input fiber and connecting fiber will affect both the visibility and phase.

Thus, with polarized illumination, measurement errors may arise from perturbations of the input lead to the MZI and connecting lead between the MZI and FBG or changes in birefringence in the MZI or FBG.

B. Illumination With Unpolarized Light

The general expression for the output intensity due to unpolarized illumination[1] is given by (A7). When the polarization eigenaxes of the MZI and FBG are parallel $(+)$ or orthogonal $(-)$, (A7) can be further simplified to

$$I_{\pm}^{\mathrm{UP}} = \frac{R}{2} I_0 \left(1 + \cos\left(\frac{\Omega_{\mathrm{MZI}}}{2} \pm \frac{\Omega_{\mathrm{FBG}}}{2}\right)\cos\Delta\phi(\bar{\lambda})\right). \quad (7)$$

The maximum and minimum visibilities are given by the term $V_{\pm} = \cos(\Omega_{\mathrm{MZI}}/2 \pm \Omega_{\mathrm{FBG}}/2)$. Thus, the birefringence in the MZI combines with the birefringence in the FBG to determine the fringe visibility. When birefringence is present in the connecting lead such that $\Omega_l \neq 0 \ (\mathrm{mod} 2\pi)$, the visibility will be within these two limits. The interferometric phase is inversely proportional to the mean wavelength $\bar{\lambda}$.

Several important conclusions can be drawn from this result. On illumination with the unpolarized light, the phase measurement is independent of the birefringence in the input fiber. In a purely birefringent sensor network with no dicroism, changes in the birefringence of the connecting lead, MZI, or FBG will only affect the fringe visibility. The interferometric phase, being inversely proportional to the mean Bragg wavelength, is therefore independent of the birefringence in the

[1]The term unpolarized light is often used to refer to light that exhibits a polarization state that changes rapidly during the observation time. In the case of natural light, these changes are random, which leads to the term randomly polarized. We use the term unpolarized to refer to light with a zero degree of polarization measured over a specified observation time.

MZI, FBG, and connecting lead. Thus, the presence of pure birefringence will not lead to measurement error when the illuminating source is unpolarized and the network free from dicroism.

C. Illumination With Partially Polarized Light

In practical systems, the degree of polarization (DOP) may not always be maintained at zero throughout the system. The broadband source may exhibit a small DOP, yielding partially polarized light, and the components making up the system may each exhibit some polarization dependent loss (PDL). If PDL is present, the DOP will change on propagation through the network. Also, if PDL is present in several components, then the total PDL at any given time will depend on the birefringence in the system at that time. Here, we consider the case of partially polarized input light and ideal components (i.e., PDL free). In this case, the amplitudes of the two orthogonal waves, given by (A5), may not be exactly matched at the detector. The output intensity for partially polarized illumination is expressed as

$$I^{\mathrm{PP}} = I_1 + x \cdot I_2 \tag{8}$$

where from the definition of the Stokes parameters, x is related to the DOP by $x = (1 - \mathrm{DOP})/(1 + \mathrm{DOP})$. Assuming that I_1 is aligned to an eigenaxis of the MZI, then summing the two intensities given by (A5) using (8) yields

$$\begin{aligned} I^{\mathrm{PP}} = \frac{R}{4} I_0 \Bigg(& 1 + x + \cos^2\left(\frac{\varphi}{2}\right) \\ & \cdot \left[\cos\left(\phi + \frac{\Omega_{\mathrm{FBG}}}{2} + \frac{\Omega_{\mathrm{MZI}}}{2}\right) \right. \\ & \left. + x \cos\left(\phi - \frac{\Omega_{\mathrm{FBG}}}{2} - \frac{\Omega_{\mathrm{MZI}}}{2}\right) \right] + \sin^2\left(\frac{\varphi}{2}\right) \\ & \cdot \left[\cos\left(\phi - \frac{\Omega_{\mathrm{FBG}}}{2} + \frac{\Omega_{\mathrm{MZI}}}{2}\right) \right. \\ & \left. + x \cos\left(\phi + \frac{\Omega_{\mathrm{FBG}}}{2} - \frac{\Omega_{\mathrm{MZI}}}{2}\right) \right] \Bigg). \end{aligned} \tag{9}$$

We consider the practical case where Ω_{MZI} is set to zero. The maximum phase error is given by the difference in measured phase when the component axes of the partially polarized light and FBG eigenaxes are parallel and orthogonal. This phase error can be determined by calculating $I_{\pm}^{\mathrm{PP}}$ for each case by setting φ to zero and π in (9), yielding

$$\begin{aligned} I_{\pm}^{\mathrm{PP}} = \frac{R}{4} I_0 \Big(& 1 + x + \left\{ 1 + 2x \cos(\Omega_{\mathrm{FBG}}) + x^2 \right\}^{\frac{1}{2}} \\ & \cdot \cos(\Delta\phi(\bar{\lambda}) + \delta) \Big) \end{aligned} \tag{10}$$

where

$$\delta_{\pm} = \tan^{-1}\left[\mathrm{DOP} \tan\left(\pm \frac{\Omega_{\mathrm{FBG}}}{2} \right) \right]. \tag{11}$$

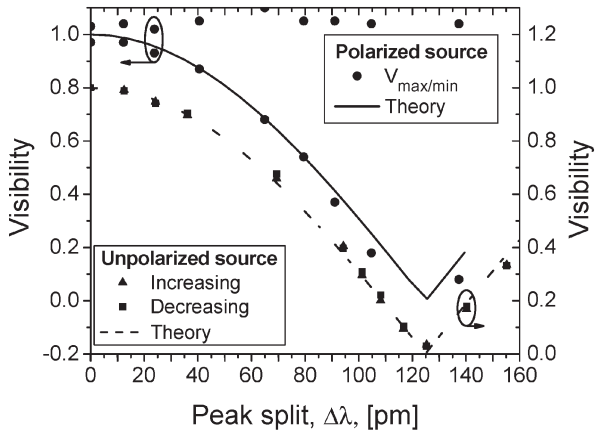

Fig. 2. Fringe visibility as a function of FBG peak splitting for a polarized and unpolarized source.

The maximum phase error is therefore given by $|\delta_+ - \delta_-|$. The measurement error drifts between the two values of δ_+ and δ_- due to changes in the birefringence in the input and connecting lead. Thus, illumination with partially polarized light will give rise to both measurement error and drift.

D. Experiment

To confirm the models presented above, the fringe visibility and phase error have been measured as a function of FBG and MZI birefringence. In the first experiment, birefringence in the MZI is minimized by replacing it with an MI with ortho-conjugate or Faraday mirrors, such that $\Omega_{\mathrm{MZI}} \cong 0(\mathrm{modulo}\ 2\pi)$. An increasing level of birefringence is generated in the FBG by applying a transverse force, using a similar method to that described in [14]. The FBG is stripped of its acrylate coating before force is applied through a loading plate. The fringe visibility is then measured as a function of applied force, using the set-up shown in Fig. 1(a). The broadband source is an erbium-doped fiber amplifier (EDFA) with a DOP less than 3%, and the Bragg grating is approximately 3 mm in length, written into SMF-28 fiber with a peak reflectivity of 1% and $\lambda_B = 1549$ nm. The peak splitting $\Delta\lambda$ of the Bragg wavelength with applied force is initially measured with an optical spectrum analyzer, and the visibility is calculated from $V = \cos(\pi n d \Delta\lambda/\bar{\lambda}^2)$, where $n = 1.465$ and $d = 6.56$ mm. The measured and calculated fringe visibilities as a function of peak splitting $\Delta\lambda$ are shown in Fig. 2. A very good agreement is obtained between the predicted and measured visibilities. The visibility is plotted for both increasing and decreasing FBG birefringence. The good repeatability obtained indicates that the FBG loading arrangement exhibits minimal hysteresis. This experiment is repeated for a polarized source by placing a polarizer at the output of the EDFA, which yielded a DOP $\sim 90\%$. In this configuration, the visibility will be given by $V = \{1 - \sin^2\varphi \sin^2(\Omega_{\mathrm{FBG}}/2)\}^{1/2}$ and, thus, will vary between the limits of unity and $\cos(\pi n d \Delta\lambda/\bar{\lambda}^2)$ depending on the birefringence in the connecting lead. This is varied using a birefringence controller placed in the connecting fiber. The visibility is extinguished when $\Omega_{\mathrm{FBG}} = 2\pi n d \Delta\lambda/\bar{\lambda}^2 = \pi(\mathrm{modulo}\ 2\pi)$.

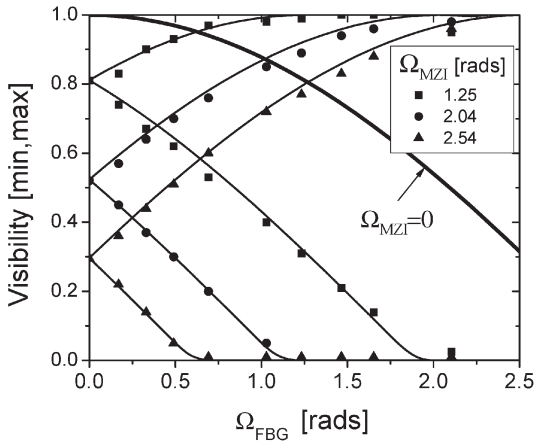

Fig. 3. Maximum and minimum visibilities as a function of Ω_{FBG} and MZI birefringence.

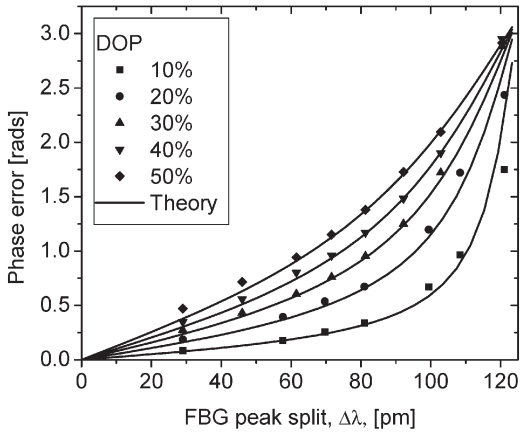

Fig. 4. Phase error versus FBG peak splitting for increasing DOP.

In the second experiment, a fixed amount of birefringence is added to the MZI using a birefringence controller placed in one arm of the MZI, when the FBG is free from birefringence and the source unpolarized. In this configuration, the fringe visibility is given by $V = \cos(\Omega_{\mathrm{MZI}}/2)$. Increasing levels of birefringence are then added to the FBG, and the limits of the fringe visibility are recorded when the birefringence in the connecting lead is changed. The result is plotted in Fig. 3 along with the limits of the fringe visibility calculated with $V = \cos(\Omega_{\mathrm{MZI}}/2 \pm \Omega_{\mathrm{FBG}}/2)$ from (7). Here, we have used $d = 3.6$ mm to calculate Ω_{FBG}. Also plotted for comparison is the curve for $\Omega_{\mathrm{MZI}} = 0$.

A very good agreement is obtained with the predicted visibility. Note that when the FBG birefringence is increased to reach the visibility limit of zero or unity, further increase in Ω_{FBG} results in this limit being maintained for certain values of connecting lead birefringence. The visibility limit is therefore not periodic and the visibility limits of zero and unity will be obtained when $\Omega_{\mathrm{MZI}}/2 \pm \Omega_{\mathrm{FBG}}/2$ equals $\pi/2$ and zero, respectively.

In the final experiment, the phase measurement error is investigated when the connecting lead is perturbed in a system when the source has a nonzero DOP. The setup is shown in Fig. 1(c). The output of the source is passed through a linear polarizer (LP) and then split into two paths with a directional coupler. The polarization state of the light in one path is changed with a polarization controller, such that on recombination, the DOP of the recombined light can be varied from zero to unity. A delay is also added to ensure that the recombined waves are mutually incoherent. The resulting DOP is monitored with a Stokes analyzer (SA). A second FBG (not shown) is added to the other output of the MZI to provide a reference phase, which will reject the phase shifts due to environmental changes of the MZI. The birefringence in the MZI is set to zero. The phase-generated carrier-demodulation method is used to extract the interferometric phase [15]. A birefringence controller is placed in the connecting lead to one of the FBGs, and the phase difference between the two FBGs is measured. As the birefringence in the FBG is increased, the maximum phase error is recorded when the birefringence in the connecting lead to the FBG is changed in a random fashion. This measurement is repeated for increasing DOP, and the result is presented in Fig. 4. The phase error predicted by (11) is also shown as solid lines in Fig. 4 calculated by $|\delta_+ - \delta_-|$, which demonstrates a good agreement.

IV. Tandem Interferometer

The model for the FBG sensor can be directly applied to the tandem-interferometer arrangement as described in Appendix B.

A. Illumination With Polarized Light

The general response of the tandem-interferometer arrangement illuminated with polarized light is given by (A3) and (A4) with Ω_{FBG} replaced with Ω_{MI}. Setting the birefringence in the MI to zero ($\Omega_{\mathrm{MI}} = 0$) yields a response given by

$$I = \frac{R}{2} I_0 \left(1 + \left\{ 1 - \sin^2\theta \sin^2\left(\frac{\Omega_{\mathrm{MZI}}}{2} \right) \right\}^{\frac{1}{2}} \times \cos\left(\phi_{\mathrm{MI}} - \gamma\right) \right) \tag{12}$$

where $\tan\gamma = \tan(\Omega_{\mathrm{MZI}}/2)\cos\theta$. Thus, the visibility and phase are dependent on the relative angle of the input SOP to the MZI and Ω_{MZI}. In this configuration, the connecting lead sensitivity is removed. This has been demonstrated in [7].

B. Illumination With Unpolarized Light

The response of the tandem interferometer to unpolarized light is given by (A7) with Ω_{FBG} replaced with Ω_{MI}. The response corresponding to when $\Re_{\mathrm{MZI}}$ is parallel $(+)$ and orthogonal $(-)$ to $\Re_{\mathrm{MI}}$ is given by

$$I_{\pm}^{\mathrm{UP}} = \frac{R}{2} I_0 \left(1 + \cos\left(\frac{\Omega_{\mathrm{MZI}}}{2} \pm \frac{\Omega_{\mathrm{MI}}}{2} \right) \cos\phi \right). \tag{13}$$

The limits of the fringe visibility are given by $V_{\pm} = \cos(\Omega_{\mathrm{MZI}}/2 \pm \Omega_{\mathrm{MI}}/2)$. Thus, as the birefringence in the

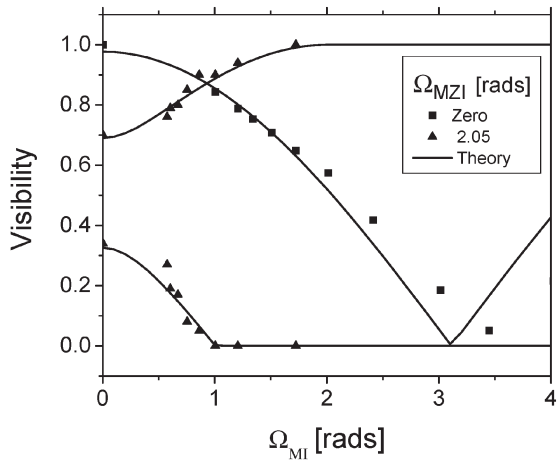

Fig. 5. Maximum and minimum visibility as a function of MI birefringence and MZI birefringence strain.

connecting lead changes, the visibility changes within the limits set by the birefringence in the MZI and MI.

C. Experiment

To confirm the validity of (13), which describes the behavior of the tandem interferometer illuminated by unpolarized light, the configuration in Fig. 1(a) is set up with the FBG replaced with the MI, and the OPD in the MZI increased to match the OPD of the MI. The MI consists of a 50:50 directional coupler fabricated with SMF28 fiber with each fiber end cleaved to provide an approximately 4% reflection and a path imbalance to match the MZI. The fiber length in each arm is approximately 26 and 32 cm. The effective OPD is a few millimeters and the bandwidth of the illuminating radiation is narrowed to 0.2 nm by reflecting it from the FBG before injection into the tandem interferometer. The birefringence in the MZI is adjusted by monitoring the fringe visibility with no birefringence added to the MI. The birefringence in the MI is increased by winding the fiber in one arm into loops to induce bend-induced birefringence [16]. The smallest loop diameter is limited by macrobending loss, so multiple loops are used to obtain large birefringence. The limits of the fringe visibility are recorded for increasing $\Omega_{\rm MI}$ and are plotted in Fig. 5 for the case of $\Omega_{\rm MZI}$ equal to zero and 2.05 rad. It was found that a small amount of intrinsic birefringence was present in the MI. This generates an initial visibility variation when the MZI birefringence is increased to 2.05 rad. This intrinsic birefringence is calculated using (13) to be $\sim$ 0.4 rad. When birefringence is added to one arm of the MI, the total birefringence is calculated by adding vectorially the two linear birefringences, such that $\Omega_{\rm MI} = \sqrt{(\Omega_{\rm intrinsic} + \Omega_{\rm bend}\cos 2\phi_b)^2 + (\Omega_{\rm bend}\sin 2\phi_b)^2}$, where $2\phi_b$ is the azimuth of the fast axis of the birefringence on the Poincaré sphere [17]. The best fit of (13) with the experimental data is obtained when $2\phi_b = \pi/2$.

V. Techniques to Overcome Lead Sensitivity

Having determined the origins of the lead sensitivity, the following techniques are demonstrated to reduce these effects.

A. Birefringence Scrambling

The sensitivity of the connecting lead between the decoding interferometer and sensor can be removed by scrambling its birefringence. This is equivalent to averaging the response over all values of φ. The response of the FBG sensor is now given by setting $\cos^2\varphi$ and $\sin^2\varphi$ equal to 1/2 in (A3) and (A7) for polarized and unpolarized light, respectively. For the case of unpolarized illumination, the visibility reduces to a constant value given by $\cos(\Omega_{\rm MZI}/2)\cos(\Omega_{\rm FBG}/2)$. Birefringence scrambling can be implemented with a polarization scrambler such as that described in [18].

B. Birefringence-Free Decoding Interferometer

Reducing the birefringence in the decoding interferometer in a system illuminated with unpolarized light will remove all the lead sensitivity, providing the system is free from dicroism. In this case, the visibility reduces to $\cos(\Omega_{\rm FBG}/2)$. If the illuminating source is partially polarized, then the visibility becomes $\{1 + 2x\cos(\Omega_{\rm FBG}) + x^2\}^{1/2}$, and the phase error is given by (11). In general, the sensor accuracy is improved with a birefringence-free decoding interferometer but it does not completely remove the lead sensitivity if the source is partially polarized or dicroism is present. The birefringence in the decoding interferometer can be nearly eliminated by incorporating ortho-conjugate mirrors into an MI.

C. Experiment

To examine the reduction in lead sensitivity using the methods described above, the effect of the lead sensitivity on the interferometric phase is measured using the following configurations based around Fig. 1(a):

1) FBG interrogated with a low-birefringence MZI;
2) FBG interrogated with a low-birefringence MZI and a birefringence scrambler (General Photonics PCS-3X) placed at the output fiber of the MZI; and
3) FBG interrogated by a birefringence-free MI with a birefringence scrambler placed at the output.

The phase error is measured by recording the phase difference between two FBGs interrogated by the same decoding interferometer, while the birefringence in the connecting lead to one FBG is changed randomly with a birefringence controller. The EDFA source is partially polarized with a DOP $\sim$ 3%, and the integration time τ_i is set to 0.1 s. The results are shown in Fig. 6. In configuration 1), the phase error is measured to be $\pm 2.1\ \mu\varepsilon$. Incorporating a birefringence scrambler yields the phase error shown in Fig. 6(b), which is reduced to $\pm 0.133\ \mu\varepsilon$. Finally, incorporating the MI reduces the phase error to less than $\pm 0.056\ \mu\varepsilon$ [Fig. 6(c)]. In this final configuration, the lead sensitivity is completely eliminated. The rms strain sensitivity is 18 nε limited by the sensor self noise.

VI. Conclusion

An analysis of the polarization properties of FBG and tandem-interferometer strain sensors, using Stokes calculus and

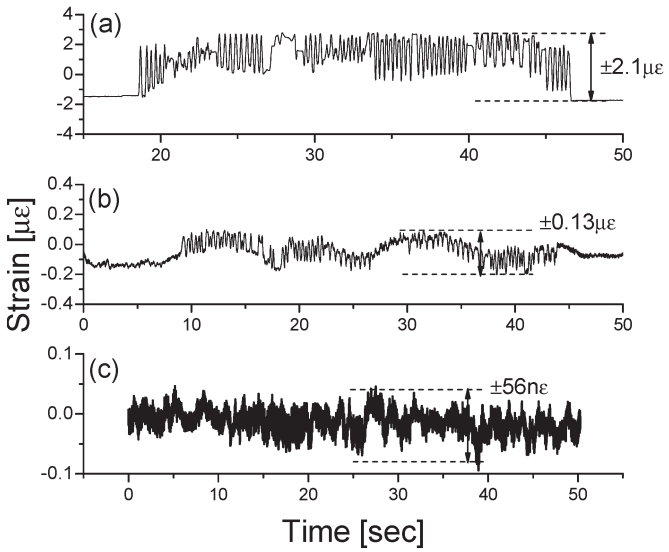

Fig. 6. Strain error due to lead sensitivity for (a) FBG interrogated with low birefringence MZI and unpolarized light, (b) same as (a) with birefringence scrambler in connecting lead, and (c) MZI replaced with birefringence-free MI and birefringence scrambler in the connecting lead.

the Poincaré sphere, has been presented. The responses of these sensors as a function of the birefringence properties of the various components, under different illuminating conditions, have been derived and confirmed with experiment. Methods to overcome the lead sensitivity based on reducing the birefringence in the decoding interferometer and birefringence scrambling are discussed and demonstrated. This has demonstrated differential strain-measurement accuracy between two FBG sensors equal to 18 $\mathrm{n}\varepsilon \cdot \mathrm{rms}$ ($\tau_i = 0.1$ s).

Appendix A
Derivation of the Response of an Interferometrically Interrogated FBG

The output intensity of the FBG sensor with a polarized source is calculated by resolving the input SOP into two orthogonal components that are coincident with the eigenaxes of the MZI. The response for each component is then calculated and the result summed to yield the overall response. The birefringence model of the network is shown schematically in Fig. 1(b). To simplify the problem, it is assumed that the birefringence in the connecting lead between the MZI and FBG, described by $\Re_l(\Omega_l)$, acts to rotate the eigenaxes of the FBG relative to the MZI. The birefringence in the FBG can be described by a Mueller matrix $\Re_{\mathrm{FBG}}(\Omega_{\mathrm{FBG}})$, where Ω_{FBG} relates to the index difference between the two birefringent axes. Thus, $\Re_l$ is set to be aligned with $\Re_{\mathrm{FBG}}$. Although this does not depict exactly the evolution of the field SOPs through the network, it simplifies the analysis of this network without loss of generality.

The birefringent Bragg grating is modeled by assigning a reflectivity and resonance wavelength for each polarization eigenaxis of the grating. Thus, the peak reflectivity for each axis is set equal to R. The resonance wavelengths for each axis are denoted λ_1 and λ_2 and the difference in Bragg resonance as $\Delta\lambda = \lambda_2 - \lambda_1$. The mean wavelength is defined as $\bar{\lambda} = (\lambda_2 + \lambda_1)/2$. The difference in Bragg resonance encountered by two orthogonal SOPs coincident with the FBG eigenaxes leads to a phase difference between them given by $2\pi n d \Delta\lambda/\bar{\lambda}^2$ when the FBG is interferometrically interrogated. This phase difference is defined as Ω_{FBG}. Thus, the relevant birefringent properties of the system are described by four parameters: Ω_{MZI} and Ω_{FBG} describe the birefringent properties of the MZI and FBG, respectively; θ is the angle subtended by the great arc joining the SOP input to the MZI, C_i, and $\Re_{\mathrm{MZI}}$; and φ is the angle subtended by the great arc joining $\Re_{\mathrm{MZI}}$ and $\Re_{\mathrm{FBG}}$ when mapped onto the Poincaré sphere. These are shown in Fig. 1(d) and (e), respectively. The response is derived by noting that two orthogonal SOPs coincident with the eigenaxes of the MZI exit with an interferometric phase difference between them equal to Ω_{MZI}. Each output SOP is then resolved into two orthogonal components coincident with the eigenaxes of the FBG. Thus, the output intensity corresponding to the two components of the input SOP are

$$\begin{aligned} I_a = \frac{R}{4} I_0 \Bigg\{ & \cos^2\left(\frac{\varphi}{2}\right)\cos^2\left(\frac{\theta}{2}\right) \\ & \times \left(1 + \cos\left(\phi(\bar{\lambda}) + \frac{\Omega_{\mathrm{FBG}}}{2} + \frac{\Omega_{\mathrm{MZI}}}{2}\right)\right) \\ & + \sin^2\left(\frac{\varphi}{2}\right)\cos^2\left(\frac{\theta}{2}\right) \\ & \times \left(1 + \cos\left(\phi(\bar{\lambda}) - \frac{\Omega_{\mathrm{FBG}}}{2} + \frac{\Omega_{\mathrm{MZI}}}{2}\right)\right)\Bigg\} \\ I_b = \frac{R}{4} I_0 \Bigg\{ & \cos^2\left(\frac{\varphi}{2}\right)\sin^2\left(\frac{\theta}{2}\right) \\ & \times \left(1 + \cos\left(\phi(\bar{\lambda}) - \frac{\Omega_{\mathrm{FBG}}}{2} - \frac{\Omega_{\mathrm{MZI}}}{2}\right)\right) \\ & + \sin^2\left(\frac{\varphi}{2}\right)\sin^2\left(\frac{\theta}{2}\right) \\ & \times \left(1 + \cos\left(\phi(\bar{\lambda}) + \frac{\Omega_{\mathrm{FBG}}}{2} - \frac{\Omega_{\mathrm{MZI}}}{2}\right)\right)\Bigg\} \end{aligned} \tag{A1}$$

where $\phi(\bar{\lambda})$ is the signal phase of interest. The output intensity is given by

$$I = I_a + I_b \tag{A2}$$

yielding

$$\begin{aligned} I = \frac{R}{2} I_0 \Bigg\{ & 1 + \cos^2\left(\frac{\varphi}{2}\right)\left\{1 - \sin^2\theta \sin^2\left(\frac{\Omega_{\mathrm{MZI}}}{2} + \frac{\Omega_{\mathrm{FBG}}}{2}\right)\right\}^{\frac{1}{2}} \\ & \times \cos\left(\phi(\bar{\lambda}) + \gamma_+\right) \\ & + \sin^2\left(\frac{\varphi}{2}\right)\left\{1 - \sin^2\theta \sin^2\left(\frac{\Omega_{\mathrm{MZI}}}{2} - \frac{\Omega_{\mathrm{FBG}}}{2}\right)\right\}^{\frac{1}{2}} \\ & \times \cos\left(\phi(\bar{\lambda}) + \gamma_-\right)\Bigg\} \end{aligned} \tag{A3}$$

where

$$\tan\gamma_{\pm} = \tan\left(\frac{\Omega_{\mathrm{MZI}}}{2} \pm \frac{\Omega_{\mathrm{FBG}}}{2}\right)\cos\theta. \tag{A4}$$

The response to an unpolarized source is derived by decomposing the input beam into two mutually incoherent orthogonal light waves [19]. The response due to each wave is given by (A3). Since the orientation of the two orthogonal components of the unpolarized light input to the MZI can be arbitrarily defined, they can be aligned to the eigenaxes of the MZI. This is equivalent to setting θ equal to zero and π in (A3) to obtain the response for each light wave

$$\begin{aligned} I_1^{\mathrm{UP}} &= \frac{R}{4}I_0\left\{1+\cos^2\left(\frac{\varphi}{2}\right)\cos\left(\phi+\frac{\Omega_{\mathrm{FBG}}}{2}+\frac{\Omega_{\mathrm{MZI}}}{2}\right)\right. \\ &\qquad \left.+\sin^2\left(\frac{\varphi}{2}\right)\cos\left(\phi-\frac{\Omega_{\mathrm{FBG}}}{2}+\frac{\Omega_{\mathrm{MZI}}}{2}\right)\right\} \\ I_2^{\mathrm{UP}} &= \frac{R}{4}I_0\left\{1+\cos^2\left(\frac{\varphi}{2}\right)\cos\left(\phi-\frac{\Omega_{\mathrm{FBG}}}{2}-\frac{\Omega_{\mathrm{MZI}}}{2}\right)\right. \\ &\qquad \left.+\sin^2\left(\frac{\varphi}{2}\right)\cos\left(\phi+\frac{\Omega_{\mathrm{FBG}}}{2}-\frac{\Omega_{\mathrm{MZI}}}{2}\right)\right\}. \end{aligned} \tag{A5}$$

Summing the two responses such that

$$I^{\mathrm{UP}} = I_1^{\mathrm{UP}} + I_2^{\mathrm{UP}} \tag{A6}$$

yields the output intensity

$$\begin{aligned} I^{\mathrm{UP}} = \frac{R}{2}I_0\left\{1+\left[\cos^2\left(\frac{\varphi}{2}\right)\cos\left(\frac{\Omega_{\mathrm{MZI}}}{2}+\frac{\Omega_{\mathrm{FBG}}}{2}\right)\right.\right. \\ \left.\left.+\sin^2\left(\frac{\varphi}{2}\right)\cos\left(\frac{\Omega_{\mathrm{MZI}}}{2}-\frac{\Omega_{\mathrm{FBG}}}{2}\right)\right]\cos\phi(\bar{\lambda})\right\}. \end{aligned} \tag{A7}$$

Appendix B
Derivation of the Response of a Tandem Interferometer

The analysis of the tandem-interferometer arrangement follows in a similar fashion to the FBG sensor. The birefringence model is shown in Fig. 1(b) with the FBG replaced with the MI. The birefringence properties of the system are now described by Ω_{MZI}, Ω_{MI}, θ, and φ. The differential birefringence in the MZI and MI are described by Ω_{MZI} and Ω_{MI}, respectively. θ is the angle subtended by the input SOP and the eigenaxis of the MZI, and φ is the angle between the eigenaxes of the MZI and MI. As before, the birefringent axis of the connecting lead $\Re_l$ is set to be parallel with $\Re_{\mathrm{MI}}$. Thus, birefringence in the connecting lead acts to rotate $\Re_{\mathrm{MI}}$ relative to $\Re_{MZI}$.

Following the same procedure as before by resolving the input SOP into two components coincident with the eigenaxes of the MZI yields

$$\begin{aligned} I_a = \frac{R}{4}I_0\left\{\cos^2\left(\frac{\varphi}{2}\right)\cos^2\left(\frac{\theta}{2}\right)\right. \\ \times\left(1+\cos\left(\phi+\frac{\Omega_{\mathrm{MI}}}{2}+\frac{\Omega_{\mathrm{MZI}}}{2}\right)\right) \\ \times\sin^2\left(\frac{\varphi}{2}\right)\cos^2\left(\frac{\theta}{2}\right) \\ \left.\times\left(1+\cos\left(\phi-\frac{\Omega_{\mathrm{MI}}}{2}+\frac{\Omega_{\mathrm{MZI}}}{2}\right)\right)\right\} \\ I_b = \frac{R}{4}I_0\left\{\cos^2\left(\frac{\varphi}{2}\right)\sin^2\left(\frac{\theta}{2}\right)\right. \\ \times\left(1+\cos\left(\phi-\frac{\Omega_{\mathrm{MI}}}{2}-\frac{\Omega_{\mathrm{MZI}}}{2}\right)\right) \\ \times\sin^2\left(\frac{\varphi}{2}\right)\sin^2\left(\frac{\theta}{2}\right) \\ \left.\times\left(1+\cos\left(\phi+\frac{\Omega_{\mathrm{MI}}}{2}-\frac{\Omega_{\mathrm{MZI}}}{2}\right)\right)\right\} \end{aligned} \tag{B1}$$

where ϕ is the phase of the MI. This is the same as (A1) with Ω_{FBG} replaced with Ω_{MI}. Thus, substituting Ω_{MI} for Ω_{FBG} in (A2)–(A7) yields the equivalent response of the tandem-interferometer arrangement.

Acknowledgment

The authors would like to thank C. Askins and A. Tveten for the very useful discussions.

References

[1] A. D. Kersey, T. A. Berkoff, and W. W. Morey, "Fiber-optic Bragg grating strain sensor with drift-compensated high-resolution interferometric wavelength-shift detection," *Opt. Lett.*, vol. 18, no. 1, pp. 72–74, Jan. 1993.

[2] G. A. Johnson, M. D. Todd, B. L. Althouse, and C. C. Chang, "Fiber Bragg grating interrogation and multiplexing with a 3 × 3 coupler and a scanning filter," *J. Lightw. Technol.*, vol. 18, no. 8, pp. 1101–1105, Aug. 2000.

[3] F. Farahi, T. P. Newson, J. D. C. Jones, and D. A. Jackson, "Coherence multiplexing of remote fibre optic Fabry–Pérot sensing system," *Opt. Commun.*, vol. 65, no. 5, pp. 319–321, Mar. 1988.

[4] G. A. Cranch, G. M. H. Flockhart, and C. K. Kirkendall, "Efficient fiber Bragg grating and fiber Fabry–Pérot sensor multiplexing scheme using a broadband, pulsed mode-locked laser," *J. Lightw. Technol.*, vol. 23, no. 11, pp. 3798–3807, Nov. 2005.

[5] R. R. Gauthier, F. Farahi, and N. Dahi, "Fiber-optic white-light interferometry: Lead sensitivity considerations," *Opt. Lett.*, vol. 19, no. 2, pp. 138–140, Jan. 1994.

[6] F. Kherbouche and B. Poumellec, "UV-induced stress field during Bragg grating inscription in optical fibres," *J. Opt. A: Pure Appl. Opt.*, vol. 3, no. 6, pp. 429–439, Nov. 2001.

[7] L. A. Ferrira, J. L. Santos, and F. Farahi, "Polarization insensitive fibre-optic white-light interferometry," *Opt. Commun.*, vol. 114, no. 5/6, pp. 386–392, Feb. 1995.

[8] E. I. Alekseev and E. N. Bazarov, "White-light interferometry with depolarization of the radiation," *Tech. Phys. Lett.*, vol. 23, no. 7, pp. 560–561, Jul. 1997.

[9] G. M. H. Flockhart, G. A. Cranch, and C. K. Kirkendall, "Differential phase tracking applied to Bragg gratings in multicore fiber for high accuracy curvature measurement," in *Proc. SPIE 6167, Symp. Smart Structures and Materials, Smart, Sensor Monitoring Systems and Applications*, San Diego, CA, Feb. 26–Mar. 2, 2006.

[10] C. D. Butter and G. B. Hocker, "Fiber optic strain gauge," *Appl. Opt.*, vol. 17, no. 18, pp. 2867–2869, Sep. 1978.
[11] H. Lefèvre, *Fiber-Optic Gyroscope*. Boston, MA: Artech House, 1993, sec. A1.7.
[12] A. D. Kersey, M. J. Marrone, A. Dandridge, and A. B. Tveten, "Optimization and stabilization of visibility in interferometric fiber-optic sensors using input-polarization control," *J. Lightw. Technol.*, vol. 6, no. 10, pp. 1599–1609, Oct. 1988.
[13] A. D. Kersey, M. J. Marrone, and A. Dandridge, "Analysis of input-polarization-induced phase noise in interferometric fiber optic sensors and its reduction using polarization scrambling," *J. Lightw. Technol.*, vol. 8, no. 6, pp. 838–845, Jun. 1990.
[14] R. B. Wagreich, W. A. Atia, H. Singh, and J. S. Sirkis, "Effects of diametric load on fibre Bragg gratings fabricated in low birefringence fibre," *Electron. Lett.*, vol. 32, no. 13, pp. 1223–1224, Jun. 1996.
[15] A. Dandridge, A. B. Tveten, and T. G. Giallorenzi, "Homodyne demodulation scheme for fiber optic sensors using phase generated carrier," *IEEE J. Quantum Electron.*, vol. QE-18, no. 10, pp. 1647–1653, Oct. 1982.
[16] R. Ulrich, S. C. Rashleigh, and W. Eickhoff, "Bending-induced birefringence in single-mode fibers," *Opt. Lett.*, vol. 5, no. 6, pp. 273–275, Jun. 1980.
[17] S. C. Rashleigh, "Origins and control of polarization effects in single-mode fibers," *J. Lightw. Technol.*, vol. LT-1, no. 2, pp. 312–330, Jun. 1983.
[18] A. D. Kersey and A. Dandridge, "Monomode fibre polarization scrambler," *Electron. Lett.*, vol. 23, no. 12, pp. 635–636, Jun. 1987.
[19] E. Hecht, *Optics*, 2nd ed. Reading, MA: Addison-Wesley, 1987, ch. 8.1.4.

Geoffrey A. Cranch received the B.Sc. degree in applied physics from the University of Bath, Somerset, U.K., in 1995 and the Ph.D. degree in applied physics, in the field of fiber-optic sensors and fiber lasers, from Heriot–Watt University, Edinburgh, U.K., in 2001.

In 1995, he joined GEC-Marconi Naval Systems (now Thales) to work on the development of fiber-optic hydrophones. In 1997, moved to the Defence Evaluation and Research Agency, Winfrith, U.K., continue his research on interferometric fiber-optic sensor systems and in fiber Bragg grating (FBG) sensors. Since 2000, he has been a Research Physicist at the Naval Research Laboratory, Washington, DC. His current research interests are in fiber laser fabrication and sensors, Bragg gratings, and interferometric sensing techniques.

Dr. Cranch is a member of the Institute of Physics, U.K., and the Optical Society of America.

Gordon M. H. Flockhart received the M.Phys. degree in optoelectronics and laser engineering and the Ph.D. degree in physics, in 1997 and 2003, respectively, from Heriot–Watt University, Edinburgh, U.K.

From 2001 to 2003, he was a Research Associate at Heriot–Watt University, investigating optical FBG-based sensors. In 2003, he joined Virginia Polytechnic Institute and State University, Blacksburg, as a Research Associate under contract from the Naval Research Laboratory, Washington, DC. Since 2004, he has been a Research Physicist with SFA, Inc., Crofton, MD, under contract from the Naval Research Laboratory's Optical Sciences Division. His research interests include low-coherence interferometry, interferometric techniques for interrogation, multiplexing, and characterization of FBGs and fiber-optic sensing systems.

Dr. Flockhart is a member of the Institute of Physics, U.K., and the Optical Society of America.

Clay K. Kirkendall (S'86–M'88) received the B.S. and M.S. degrees in electrical engineering from George Mason University, Fairfax, VA, in 1987 and 1991, respectively.

He developed fiber-optic communication and sensor systems at Dylor Corporation, Fairfax, from 1987 to 1991 before joining the Optical Sciences Division at the Naval Research Laboratory, Washington, D.C., in 1991. He has participated in the development and field-testing of many fiber-optic sensor systems, such as magnetic sensor arrays, fixed acoustic arrays, and towed arrays. His interests include transducer design, optical interrogation, fiber-optic sensor multiplexing, interferometric demodulation schemes, and polarization-diversity receiver approaches.

Mr. Kirkendall is currently the Head of the Fiber Optic Acoustic Sensor Section at the Naval Research Laboratory (NRL) and is responsible for the research and development efforts in the area of interferometric-based fiber-optic sensing.